# High-order *S*-matrix theory of atomic nonsequential double ionization in intense laser fields

Xinyan Jia,[1] Li Guo,[2,*] Xiaolei Hao,[3] Wilhelm Becker,[4] and Jing Chen[5,6,†]

[1]*School of Physical Science and Technology, Southwest Jiaotong University, Chengdu 610031, China*
[2]*Department of Physics, Shanghai Normal University, Shanghai 200234, China*
[3]*Institute of Theoretical Physics and Department of Physics, Shanxi University, Taiyuan 030006, China*
[4]*Max-Born-Institut, Max-Born-Strasse 2a, 12489 Berlin, Germany*
[5]*Hefei National Laboratory, and Hefei National Research Center for Physical Sciences at the Microscale and School of Physical Sciences, University of Science and Technology of China, Hefei 230026, China*
[6]*Shenzhen Key Laboratory of Ultraintense Laser and Advanced Material Technology, Center for Advanced Material Diagnostic Technology, and College of Engineering Physics, Shenzhen Technology University, Shenzhen 518118, China*

(Received 27 June 2023; revised 22 November 2023; accepted 3 January 2024; published 5 February 2024)

Coulomb corrections to the conventional strong-field approximation (SFA) theory (the lowest-order term of the *S*-matrix expansion) for nonsequential double ionization are considered by calculating higher-order terms of the *S*-matrix expansion that take into account multiple Coulomb interactions of the first-ionized electron with the ionic core while the second electron is still in its ground state. For a Ne atom in a linearly polarized laser field, the distribution of the components of the final electron momenta parallel to the field polarization is presented based on the *S*-matrix expansion up to the sixth order, which involves up to four Coulomb interactions between the parent ion and the first-ionized electron before it collides with the second bound electron. The calculated electron momentum distribution is significantly modified compared with the outcome of the conventional SFA. It is consistent with experimental results and a semiclassical simulation that fully takes into account the effect of the Coulomb potential on the first-tunneled electron. Our analysis shows that multiple Coulomb interactions of the first-ionized electron with the ionic core significantly modify the distribution of the final momenta by favoring larger and nearly equal momenta, in line with experimental results and semiclassical simulations.

DOI: 10.1103/PhysRevA.109.023105

## I. INTRODUCTION

Among the nonlinear phenomena displayed by atoms subjected to intense laser fields [1–4], nonsequential double ionization (NSDI), as one of the most fundamental and significant processes that involve electron correlation, has been intensely studied over the past few decades [4–6]. After a long debate about its underlying mechanism [7–10], the cold target recoil ion momentum spectroscopy technique [11] provided decisive experimental evidence of the dominance of the rescattering mechanism in atomic NSDI [12–15] and paved the way towards the acquisition of a wealth of information about the electron-electron correlation in the double-ionization process. Experimental measurements of the full two-electron momentum correlation distributions have shown that, within a certain range of field intensity, both of the liberated electrons in atomic NSDI are mainly emitted into the same hemisphere, which has consolidated the dominant contribution of the rescattering mechanism [16–20]. Now it is commonly accepted that rescattering is the main physical mechanism responsible for NSDI [8].

In this picture, one of the valence electrons is liberated from its parent ion by tunneling ionization. This electron may be driven back by the laser field into an inelastic collision with its parent ion. If the energy thereby transferred to the second electron is higher than its ionization potential, the second electron will be ionized directly. This process is called recollision-impact ionization. If the transferred energy is not sufficient to free the second electron, it may be pumped into an excited state from which it may be liberated by the external laser field at a later time. This is referred to as recollision excitation with subsequent ionization (RESI) [17,21]. Later, fingerlike structures were observed in the electron-electron correlation distribution and attributed to the postcollision Coulomb interaction between the two electrons [22–27]. In addition, interference effects have been revealed in the RESI channel in 800-nm [28–30] and 2400-nm laser fields [31]. More recently, recollision of the second electron with the ion is also found to play an important role in the NSDI process [32].

Traditional perturbation theory with respect to the laser field fails to describe the nonlinear phenomena of strong-field physics. Various nonperturbative approaches have been developed, such as numerical solution of the time-dependent Schrödinger equation [33], semiclassical models [34–36], completely classical models [37], and models based on particular Feynman diagrams and the strong-field approximation (SFA) [10,21,38–41]. The SFA theory has the advantage of requiring a relatively small calculational effort and providing a clear physical picture. Various atomic and molecular processes in intense laser fields have been well described by theories based on the SFA, in which the interaction between

*guoli@shnu.edu.cn
†chenjing@ustc.edu.cn

 

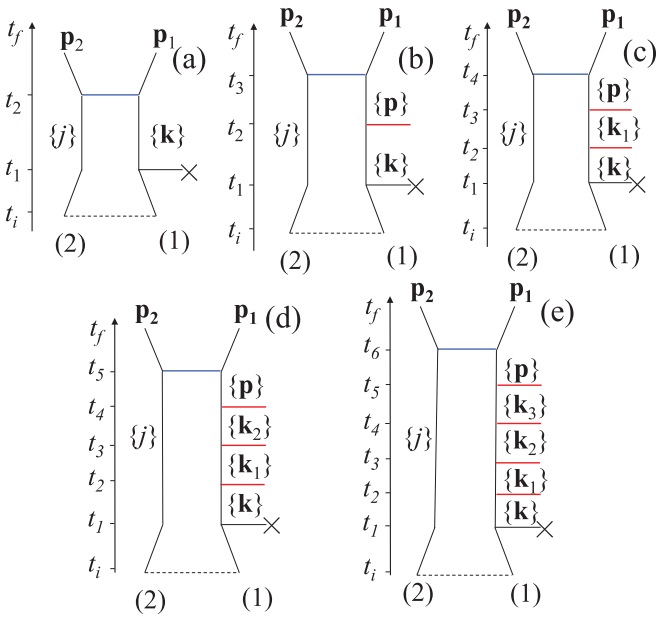


FIG. 1. Feynman diagrams of nonsequential double ionization for the (a) second-order, (b) third-order, (c) fourth-order, (d) fifth-order, and (e) sixth-order terms of the $S$-matrix expansion. In these diagrams, the dashed line at the initial time stands for the electron-electron correlation in the initial ground state of the atom, the notation—× represents the initial interaction with the laser field that liberates the first electron, the horizontal (blue) line between the two electron lines denotes the electron-electron interaction, and the short (red) horizontal lines represent the Coulomb interactions of the first-liberated electron with the core. Time goes up as indicated. All electron lines describing liberated electrons correspond to Volkov states.

the external laser field and the electron is treated nonperturbatively [5,42–45]. However, such theories ignore the effect of the Coulomb potential of the parent ion on the emitted electron after it has been freed. The low-energy structure (LES) [46–50] and the zero-energy structure [51] in the photoelectron momentum distribution of above-threshold ionization are accessible to the SFA [52]. However, the surprising magnitude of the LES, which for long wavelengths dominates the spectrum at very low energies, is caused by the Coulomb potential, which dramatically enhances the formation of these peculiar structures [48–50,52–59].

In the quantum description, i.e., the SFA theory of NSDI, work so far has focused on the lowest-order Feynman diagram, which is presented in Fig. 1(a). It describes the first electron being lifted by the laser field into the continuum and propagating in its presence up to a recollision with the second (up to this time bound) electron, which is liberated in this process. Thereafter, both electrons continue to propagate in the field towards the detector. All interactions with the laser field are incorporated exactly to all orders via the Volkov solution [5,10,38]. The mutual Coulomb interaction of the two final electrons can be and has been included [24,27,40]. However, the presence of the ionic core enters this formalism only via the initial bound state of the second electron. In reality, both electrons, once in the continuum, will interact not only with one another but also with the ionic core. This leads to a multitude of diagrams that describe the electrons Coulomb interacting with the core. For example, one collision between both electrons and the ionic core after they are ionized is taken into account in the third-order term [60]. (In earlier work, the second-ionizing electron-electron collision was sometimes simulated by a contact interaction, which was interpreted as an effective interaction that includes the Coulomb potential of the ion [40].) Another class of diagrams that we disregard describes the aforementioned process of rescattering excitation with subsequent ionization where the recolliding electron promotes the bound electron to an excited state, which is ionized at a later time (see, e.g., the review in [5]). For neon, the excited states of the singly charged ion are comparatively high in energy. Hence, for neon, neglecting the RESI diagrams may be better justified than, e.g., for argon. In this paper we evaluate up to four additional Coulomb interactions of the first electron with the core while it is in the continuum, preceding the crucial second-ionizing electron-electron interaction. The core is treated as one Coulomb center including the second electron, which is still bound. We make no claim that these higher-order diagrams are the most important high-order diagrams. Rather, their calculation allows us to assess the characteristic modifications in the electron momentum correlation distribution that occur if one proceeds order by order in the $S$-matrix expansion [cf. Figs. 1(b)–1(e)]. Physically, these diagrams correspond to repeated interactions of the first-ionized electron with the core. For a short-range or a contact potential, due to their short range, the interaction has to occur when the electron returns to the core, so the interactions correspond to recollisions and their significance quickly diminishes owing to wave-packet spreading. However, for a long-range Coulomb potential the interaction between the Coulomb potential and the first electron can actually occur at any time and at any distance from the ion during the evolution of the photoelectron, so it may or may not correspond to a recollision [56]. Therefore, the higher-order diagrams also include Coulomb focusing, which counteracts spreading [61,62]. It will then turn out that the higher-order diagrams significantly modify the electron-electron correlation distribution obtained by the lowest-order correlation diagram.

We leave aside the question of the convergence of the corresponding series. In fact, our results strongly suggest that the Dyson series for the double-ionization amplitude does not converge. A corresponding problem occurs in the much simpler case of field-free electron scattering off a Coulomb potential where it is well understood. In this case, all diagrams higher than first order diverge, but the series can be summed up and all divergencies enter a divergent phase factor. This drops out of the scattering cross section, which becomes identical to the first-order result. A similar problem also occurs in the SFA description of the so-called low-energy structure in above-threshold ionization [53]: The lowest-order rescattering diagram yields a good description. According to our calculations, higher orders appear to preserve the shape of the lowest-order ionization rate while they increasingly enhance its magnitude. This suggests that the series fails to converge [63].

The approach that we pursue in this paper, viz., including increasingly higher orders of the Coulomb potential in an

$S$-matrix expansion, should be seen in contrast to nonperturbative avenues that include the Coulomb potential in the action, which might be subsumed under the Coulomb quantum-orbit strong-field approximation (see, e.g., [64]).

This paper is arranged as follows. In Sec. II the high-order $S$-matrix theory is presented. Then we apply the theory to study the electron-electron momentum correlation distribution of NSDI for a Ne atom. The results are presented and discussed in Sec. III. We summarize and give our main conclusions in Sec. IV. The Appendix briefly presents the corresponding $S$-matrix expansion for above-threshold ionization.

## II. THEORY

We study the nonsequential-double-ionization process of the Ne atom by applying the Dyson expansion of the $S$ matrix up to sixth order, which takes into account the Coulomb interaction between the parent ion and the first-ionized electron up to four times in between its liberation and its collision with the second (up to this time bound) active electron. The corresponding Feynman diagrams are presented in Fig. 1. Within our approximation of two active electrons, the pertinent transition amplitudes are

$$A_{fi}^{(3)}(\mathbf{p}_1,\mathbf{p}_2)=(-i)^3\int_{-\infty}^{\infty}dt_3\int_{-\infty}^{t_3}dt_2\int_{-\infty}^{t_2}dt_1\int d\mathbf{p}\int d\mathbf{k}\big\langle\psi_{\mathbf{p}_2}^{(V)}(\mathbf{r}_2,t_3)\psi_{\mathbf{p}_1}^{(V)}(\mathbf{r}_1,t_3)\big|V_{12}\big|\psi_j^{+}(\mathbf{r}_2,t_3)\psi_{\mathbf{p}}^{(V)}(\mathbf{r}_1,t_3)\big\rangle$$
$$\times\big\langle\psi_{\mathbf{p}}^{(V)}(\mathbf{r}_1,t_2)\big|V_C\big|\psi_{\mathbf{k}}^{(V)}(\mathbf{r}_1,t_2)\big\rangle\big\langle\psi_j^{+}(\mathbf{r}_2,t_1)\psi_{\mathbf{k}}^{(V)}(\mathbf{r}_1,t_1)\big|V_L(t_1)\big|\Psi_i(\mathbf{r}_1,\mathbf{r}_2,t_1)\big\rangle, \tag{1}$$

$$A_{fi}^{(4)}(\mathbf{p}_1,\mathbf{p}_2)=(-i)^4\int_{-\infty}^{\infty}dt_4\int_{-\infty}^{t_4}dt_3\int_{-\infty}^{t_3}dt_2\int_{-\infty}^{t_2}dt_1\int d\mathbf{p}\int d\mathbf{k}_1\int d\mathbf{k}\big\langle\psi_{\mathbf{p}_2}^{(V)}(\mathbf{r}_2,t_4)\psi_{\mathbf{p}_1}^{(V)}(\mathbf{r}_1,t_4)\big|V_{12}\big|\psi_j^{+}(\mathbf{r}_2,t_4)\psi_{\mathbf{p}}^{(V)}(\mathbf{r}_1,t_4)\big\rangle$$
$$\times\big\langle\psi_{\mathbf{p}}^{(V)}(\mathbf{r}_1,t_3)\big|V_C\big|\psi_{\mathbf{k}_1}^{(V)}(\mathbf{r}_1,t_3)\big\rangle\big\langle\psi_{\mathbf{k}_1}^{(V)}(\mathbf{r}_1,t_2)\big|V_C\big|\psi_{\mathbf{k}}^{(V)}(\mathbf{r}_1,t_2)\big\rangle\big\langle\psi_j^{+}(\mathbf{r}_2,t_1)\psi_{\mathbf{k}}^{(V)}(\mathbf{r}_1,t_1)\big|V_L(t_1)\big|\Psi_i(\mathbf{r}_1,\mathbf{r}_2,t_1)\big\rangle, \tag{2}$$

$$A_{fi}^{(5)}(\mathbf{p}_1,\mathbf{p}_2)=(-i)^5\int_{-\infty}^{\infty}dt_5\int_{-\infty}^{t_5}dt_4\int_{-\infty}^{t_4}dt_3\int_{-\infty}^{t_3}dt_2\int_{-\infty}^{t_2}dt_1\int d\mathbf{p}\int d\mathbf{k}_2\int d\mathbf{k}_1\int d\mathbf{k}$$
$$\times\big\langle\psi_{\mathbf{p}_2}^{(V)}(\mathbf{r}_2,t_5)\psi_{\mathbf{p}_1}^{(V)}(\mathbf{r}_1,t_5)\big|V_{12}\big|\psi_j^{+}(\mathbf{r}_2,t_5)\psi_{\mathbf{p}}^{(V)}(\mathbf{r}_1,t_5)\big\rangle\big\langle\psi_{\mathbf{p}}^{(V)}(\mathbf{r}_1,t_4)\big|V_C\big|\psi_{\mathbf{k}_2}^{(V)}(\mathbf{r}_1,t_4)\big\rangle\big\langle\psi_{\mathbf{k}_2}^{(V)}(\mathbf{r}_1,t_3)\big|V_C\big|\psi_{\mathbf{k}_1}^{(V)}(\mathbf{r}_1,t_3)\big\rangle$$
$$\times\big\langle\psi_{\mathbf{k}_1}^{(V)}(\mathbf{r}_1,t_2)\big|V_C\big|\psi_{\mathbf{k}}^{(V)}(\mathbf{r}_1,t_2)\big\rangle\big\langle\psi_j^{+}(\mathbf{r}_2,t_1)\psi_{\mathbf{k}}^{(V)}(\mathbf{r}_1,t_1)\big|V_L(t_1)\big|\Psi_i(\mathbf{r}_1,\mathbf{r}_2,t_1)\big\rangle, \tag{3}$$

and

$$A_{fi}^{(6)}(\mathbf{p}_1,\mathbf{p}_2)=(-i)^6\int_{-\infty}^{\infty}dt_6\int_{-\infty}^{t_6}dt_5\int_{-\infty}^{t_5}dt_4\int_{-\infty}^{t_4}dt_3\int_{-\infty}^{t_3}dt_2\int_{-\infty}^{t_2}dt_1\int d\mathbf{p}\int d\mathbf{k_3}\int d\mathbf{k}_2\int d\mathbf{k}_1\int d\mathbf{k}$$
$$\times\big\langle\psi_{\mathbf{p}_2}^{(V)}(\mathbf{r}_2,t_6)\psi_{\mathbf{p}_1}^{(V)}(\mathbf{r}_1,t_6)\big|V_{12}\big|\psi_j^{+}(\mathbf{r}_2,t_6)\psi_{\mathbf{p}}^{(V)}(\mathbf{r}_1,t_6)\big\rangle\big\langle\psi_{\mathbf{p}}^{(V)}(\mathbf{r}_1,t_5)\big|V_C\big|\psi_{\mathbf{k}_3}^{(V)}(\mathbf{r}_1,t_5)\big\rangle$$
$$\times\big\langle\psi_{\mathbf{k}_3}^{(V)}(\mathbf{r}_1,t_4)\big|V_C\big|\psi_{\mathbf{k}_2}^{(V)}(\mathbf{r}_1,t_4)\big\rangle\big\langle\psi_{\mathbf{k}_2}^{(V)}(\mathbf{r}_1,t_3)\big|V_C\big|\psi_{\mathbf{k}_1}^{(V)}(\mathbf{r}_1,t_3)\big\rangle\big\langle\psi_{\mathbf{k}_1}^{(V)}(\mathbf{r}_1,t_2)\big|V_C\big|\psi_{\mathbf{k}}^{(V)}(\mathbf{r}_1,t_2)\big\rangle$$
$$\times\big\langle\psi_j^{+}(\mathbf{r}_2,t_1)\psi_{\mathbf{k}}^{(V)}(\mathbf{r}_1,t_1)\big|V_L(t_1)\big|\Psi_i(\mathbf{r}_1,\mathbf{r}_2,t_1)\big\rangle. \tag{4}$$

Here the angular brackets denote matrix elements of the interaction operators, which will be evaluated in position space. The wave function of the initial atomic ground state with binding energy $E_i=-I_{p_1}-I_{p_2}<0$ is $\Psi_i(\mathbf{r}_1,\mathbf{r}_2,t)=\exp(-iE_it)\phi_i(\mathbf{r}_1)\phi_i(\mathbf{r}_2)$, while $\psi_j^{+}(\mathbf{r}_2,t)=\exp(-iE_jt)\phi_j^{+}(\mathbf{r}_2)$ is the ground-state wave function of the residual ion with binding energy $E_j=-I_{p_2}<0$ ($I_{p_1}$ and $I_{p_2}$ are the ionization potentials of the first and the second electron, respectively). The plane-wave Volkov state is $\psi_{\mathbf{k}}^{(V)}(\mathbf{r},t)=\phi_{\mathbf{k}}(\mathbf{r})\exp\{-i\int^t d\tau[\mathbf{k}+\mathbf{A}(\tau)]^2/2\}$, with $\phi_{\mathbf{k}}(\mathbf{r})=\exp(i\mathbf{k}\cdot\mathbf{r})/v^{1/2}$, where $v$ is the normalization volume. The laser-electron interaction in the velocity gauge, the binding potential of the first-ionized electron, and the Coulomb interaction between the two active electrons are

$$V_L(t)=\mathbf{p}\cdot\mathbf{A}(t)+\mathbf{A}^2(t)/2,$$
$$V_C=-\frac{Z_{\rm eff}}{r_1},$$
$$V_{12}=\frac{1}{|\mathbf{r}_1-\mathbf{r}_2|}, \tag{5}$$

respectively, where $\mathbf{A}(t)$ is the vector potential of the laser field; in the following we restrict ourselves to the linearly polarized field $\mathbf{A}(t)=A_0\boldsymbol{\varepsilon}\cos\omega t$, with $A_0$ the amplitude, $\boldsymbol{\varepsilon}$ the unit polarization vector, and $\omega$ the frequency of the field. The effective charge of the $Ne^+$ ion is defined as $Z_{\rm eff}=\sqrt{2I_{p_1}}$. The

physical significance of the third- to sixth-order terms (1)–(4) of the $S$-matrix expansion is illustrated by the corresponding Feynman diagrams of Fig. 1. At the initial time, the two active electrons are in the atomic ground state; at the later time $t_1$ one of the electrons (labeled 1) interacts with the laser field and is freed, absorbing a large number of photons in the process. This emitted electron may return to and Coulomb interact with the atomic core once, twice, three times, or four times until finally it interacts with the second active electron and kicks it out so that the electrons emerge in the continuum with the final momenta $\mathbf{p}_1$ and $\mathbf{p}_2$.

In our calculation, we employ the Jacobi-Anger formula to expand the Volkov wave functions $\psi_{\mathbf{k}}^{(V)}(\mathbf{r}, t)$ in terms of Bessel functions, which allows us to perform the multiple time integrations exactly, yielding the $\delta$ function for overall momentum conservation in Eq. (6) and the energy denominators in Eqs. (9)–(12). The differential rates of nonsequential double ionization due to absorption of $N$ photons then can be written as

$$\frac{dW^{(N)}(\mathbf{p}_1, \mathbf{p}_2)}{d\mathbf{p}_1 d\mathbf{p}_2} = 2\pi\delta\left(\frac{p_1^2}{2} + \frac{p_2^2}{2} + I_{p_1} + I_{p_2} + 2U_p - N\omega\right)\left|T^{(N)}(\mathbf{p}_1, \mathbf{p}_2)\right|^2, \tag{6}$$

where

$$T^{(N)}(\mathbf{p}_1, \mathbf{p}_2) = \frac{v}{(2\pi)^3}\sum_M \int d\mathbf{p}\, V_{\mathbf{p}_2\mathbf{p}_1,j\mathbf{p}} V_{j,i} J_{N-M}\left(\boldsymbol{\alpha}\cdot(\mathbf{p}_1 + \mathbf{p}_2 - \mathbf{p}), -\frac{z}{2}\right) T^{(M)}(\mathbf{p}), \tag{7}$$

with

$$\begin{aligned} V_{\mathbf{p}_2\mathbf{p}_1,j\mathbf{p}} &= \langle\phi_{\mathbf{p}_1}(\mathbf{r}_1)\phi_{\mathbf{p}_2}(\mathbf{r}_2)|V_{12}|\phi_j^+(\mathbf{r}_2)\phi_{\mathbf{p}}(\mathbf{r}_1)\rangle, \\ V_{j,i} &= \langle\phi_j^+(\mathbf{r}_2)|\phi_i(\mathbf{r}_2)\rangle. \end{aligned} \tag{8}$$

The quantities $T^{(M)}(\mathbf{p})$ combine the various matrix elements. To third, fourth, fifth, and sixth order they are

$$T_3^{(M)}(\mathbf{p}) = i\frac{v}{(2\pi)^3}\int d\mathbf{k}\sum_n \langle\phi_{\mathbf{p}}(\mathbf{r}_1)|V_C|\phi_{\mathbf{k}}(\mathbf{r}_1)\rangle\langle\phi_{\mathbf{k}}(\mathbf{r}_1)|\phi_i(\mathbf{r}_1)\rangle(U_p - n\omega)\frac{J_{M-n}(\boldsymbol{\alpha}\cdot(\mathbf{p}-\mathbf{k}))}{p^2/2 + I_{p_1} + U_p - M\omega}\frac{J_n(\boldsymbol{\alpha}\cdot\mathbf{k}, -\frac{z}{2})}{k^2/2 + I_{p_1} + U_p - n\omega}, \tag{9}$$

$$\begin{aligned} T_4^{(M)}(\mathbf{p}) = \frac{v^2}{(2\pi)^6}\int d\mathbf{k}_1 \int d\mathbf{k}\sum_{n_1}\sum_n &\langle\phi_{\mathbf{p}}(\mathbf{r}_1)|V_C|\phi_{\mathbf{k}_1}(\mathbf{r}_1)\rangle\langle\phi_{\mathbf{k}_1}(\mathbf{r}_1)|V_C|\phi_{\mathbf{k}}(\mathbf{r}_1)\rangle\langle\phi_{\mathbf{k}}(\mathbf{r}_1)|\phi_i(\mathbf{r}_1)\rangle \\ &\times (U_p - n\omega)\frac{J_{M-n-n_1}(\boldsymbol{\alpha}\cdot(\mathbf{p}-\mathbf{k}_1))}{p^2/2 + I_{p_1} + U_p - M\omega}\frac{J_{n_1}(\boldsymbol{\alpha}\cdot(\mathbf{k}_1-\mathbf{k}))}{k_1^2/2 + I_{p_1} + U_p - (n+n_1)\omega}\frac{J_n(\boldsymbol{\alpha}\cdot\mathbf{k}, -\frac{z}{2})}{k^2/2 + I_{p_1} + U_p - n\omega}, \end{aligned} \tag{10}$$

$$\begin{aligned} T_5^{(M)}(\mathbf{p}) = -i\frac{v^3}{(2\pi)^9}\int d\mathbf{k}_2 \int d\mathbf{k}_1 \int d\mathbf{k}\sum_{n_2}\sum_{n_1}\sum_n &\langle\phi_{\mathbf{p}}(\mathbf{r}_1)|V_C|\phi_{\mathbf{k}_2}(\mathbf{r}_1)\rangle\langle\phi_{\mathbf{k}_2}(\mathbf{r}_1)|V_C|\phi_{\mathbf{k}_1}(\mathbf{r}_1)\rangle \\ &\times \langle\phi_{\mathbf{k}_1}(\mathbf{r}_1)|V_C|\phi_{\mathbf{k}}(\mathbf{r}_1)\rangle\langle\phi_{\mathbf{k}}(\mathbf{r}_1)|\phi_i(\mathbf{r}_1)\rangle(U_p - n\omega)\frac{J_{M-n-n_1-n_2}(\boldsymbol{\alpha}\cdot(\mathbf{p}-\mathbf{k}_2))}{p^2/2 + I_{p_1} + U_p - M\omega} \\ &\times \frac{J_{n_2}(\boldsymbol{\alpha}\cdot(\mathbf{k}_2-\mathbf{k}_1))}{k_2^2/2 + I_{p_1} + U_p - (n+n_1+n_2)\omega}\frac{J_{n_1}(\boldsymbol{\alpha}\cdot(\mathbf{k}_1-\mathbf{k}))}{k_1^2/2 + I_{p_1} + U_p - (n+n_1)\omega}\frac{J_n(\boldsymbol{\alpha}\cdot\mathbf{k}, -\frac{z}{2})}{k^2/2 + I_{p_1} + U_p - n\omega}, \end{aligned} \tag{11}$$

and

$$\begin{aligned} T_6^{(M)}(\mathbf{p}) = -\frac{v^4}{(2\pi)^{12}}\int d\mathbf{k}_3 \int d\mathbf{k}_2 \int d\mathbf{k}_1 \int d\mathbf{k}\sum_{n_3}\sum_{n_2}\sum_{n_1}\sum_n &\langle\phi_{\mathbf{p}}(\mathbf{r}_1)|V_C|\phi_{\mathbf{k}_3}(\mathbf{r}_1)\rangle \\ &\times \langle\phi_{\mathbf{k}_3}(\mathbf{r}_1)|V_C|\phi_{\mathbf{k}_2}(\mathbf{r}_1)\rangle\langle\phi_{\mathbf{k}_2}(\mathbf{r}_1)|V_C|\phi_{\mathbf{k}_1}(\mathbf{r}_1)\rangle\langle\phi_{\mathbf{k}_1}(\mathbf{r}_1)|V_C|\phi_{\mathbf{k}}(\mathbf{r}_1)\rangle\langle\phi_{\mathbf{k}}(\mathbf{r}_1)|\phi_i(\mathbf{r}_1)\rangle(U_p - n\omega) \\ &\times \frac{J_{M-n-n_1-n_2-n_3}(\boldsymbol{\alpha}\cdot(\mathbf{p}-\mathbf{k}_3))}{p^2/2 + I_{p_1} + U_p - M\omega}\frac{J_{n_3}(\boldsymbol{\alpha}\cdot(\mathbf{k}_3-\mathbf{k}_2))}{k_3^2/2 + I_{p_1} + U_p - (n+n_1+n_2+n_3)\omega} \\ &\times \frac{J_{n_2}(\boldsymbol{\alpha}\cdot(\mathbf{k}_2-\mathbf{k}_1))}{k_2^2/2 + I_{p_1} + U_p - (n+n_1+n_2)\omega}\frac{J_{n_1}(\boldsymbol{\alpha}\cdot(\mathbf{k}_1-\mathbf{k}))}{k_1^2/2 + I_{p_1} + U_p - (n+n_1)\omega}\frac{J_n\left(\boldsymbol{\alpha}\cdot\mathbf{k}, -\frac{z}{2}\right)}{k^2/2 + I_{p_1} + U_p - n\omega}. \end{aligned} \tag{12}$$

The generalized Bessel function of two arguments is defined as

$$J_m(a, b) = \sum_{n=-\infty}^{\infty} J_{m-2n}(a)J_n(b) \tag{13}$$

and $z = U_p/\omega$, $\boldsymbol{\alpha} = A_0\boldsymbol{\varepsilon}/\omega$ denotes the electron quiver motion vector in the laser field, and $U_p = A_0^2/4$ is the ponderomotive energy of the electron in the laser field.

For single ionization, the analog of the delta function in Eq. (6) is $\delta(p^2/2 + I_{p_1} + U_p - M\omega)$, where the integer $M =$

$m_0 + l$ denotes the number of photons absorbed from the field with $m_0 = [(I_{p_1} + U_p)/\omega]_{\rm int}$ the minimum number required to overcome the ionization potential ($[x]_{\rm int}$ is the smallest integer greater than or equal to $x$) and $l = 1, 2, 3, \ldots$ the number of additional photons absorbed.

For double ionization, the analogous photon number is $N = n_0 + m = [(I_{p_1} + I_{p_2} + 2U_p)/\omega]_{\rm int} + m$. The photon numbers $M$ in Eqs. (9)–(12) are equal to $n + n_1$, $n + n_1 + n_2$, $n + n_1 + n_2 + n_3$, and $n + n_1 + n_2 + n_3 + n_4$, respectively, where $n$ is the number of photons absorbed from the field when the first electron is liberated into the continuum and $n_1$, $n_2$, $n_3$, and $n_4$ count the photons absorbed in its subsequent (first, second, third, and fourth) Coulomb scatterings off the core. The photon numbers $n_i$ can be positive or negative, corresponding to absorption of photons from the laser field ($n_i > 0$) or emission into the field ($n_i < 0$). For the later discussion, we note that the number $m$ of excess photons determines the kinetic energy left for the final electrons.

In Eqs. (7) and (9)–(12) the integrations over the intermediate momenta $\mathbf{k}$, $\mathbf{k}_1$, $\mathbf{k}_2$, $\mathbf{k}_3$, and $\mathbf{p}$ remain to be carried out. We recall that the energy denominators in Eqs. (9)–(12) all have a small positive imaginary part $i\epsilon$ with $\epsilon > 0$, which was introduced to enforce convergence of the temporal integrations at their upper limits. For the integrations over the absolute values $k$, $k_1$, $k_2$, $k_3$, and $p$ we then invoke the so-called pole approximation [65], which consists in using the generalized function

$$\lim_{\epsilon \to 0} \frac{1}{x + i\epsilon} = P\frac{1}{x} - i\pi\delta(x), \tag{14}$$

where $P$ denotes the principal part, and keeping only the $\delta$ function. For example, for the third-order contribution we have

$$\lim_{\epsilon \to 0} \int_{-\infty}^{\infty} \frac{f(k)d(k^2/2)}{(k^2/2 + I_{p_1} + U_p - n\omega) + i\epsilon} \approx -i\pi f(k_n), \tag{15}$$

with $k_n = \sqrt{2(n\omega - I_{p_1} - U_p)}$. The remaining integrations over the angular components of the momenta $\mathbf{k}$, $\mathbf{k}_1$, $\mathbf{k}_2$, $\mathbf{k}_3$, and $\mathbf{p}$ then are calculated numerically. All spatial integrations in Eqs. (8)–(12), which are denoted by the angular brackets, are performed analytically.

The momentum distributions of the two electrons parallel to the polarization direction are obtained by integrating the differential ionization rate (6) over the final-momentum components perpendicular to the laser-field polarization

$$\frac{dW}{dp_1^{\parallel} dp_2^{\parallel}} = \sum_N \int \frac{dW^{(N)}(\mathbf{p}_1, \mathbf{p}_2)}{d\mathbf{p}_1 d\mathbf{p}_2} p_1^{\perp} p_2^{\perp} dp_1^{\perp} dp_2^{\perp} d\varphi_1 d\varphi_2, \tag{16}$$

where $p_i^{\parallel}$ and $p_i^{\perp}$ denote the components of $\mathbf{p}_i$ parallel and perpendicular to the laser polarization axis and $\varphi_1$ and $\varphi_2$ are the azimuthal angles, which vary between 0 and $2\pi$.

## III. CALCULATIONS AND DISCUSSION

We first show the results obtained from the $S$-matrix expansion (16) up to sixth order, which incorporate up to four interactions between the first-ionized electron and the ionic Coulomb potential. Initially, the Ne atom is in the $2p_z$ ground state and it is ionized by a linearly polarized laser field with intensity $1.05 \times 10^{15}$ W/cm$^2$ and wavelength 800 nm. The corresponding ionization potentials of the ground states of the Ne atom and its ion are $I_{p_1} = 0.7928$ a.u. and $I_{p_2} = 1.506$ a.u., respectively. Here we assume that the initial state has the magnetic quantum number $m = 0$, since this is known to generally dominate the ionization process [66].

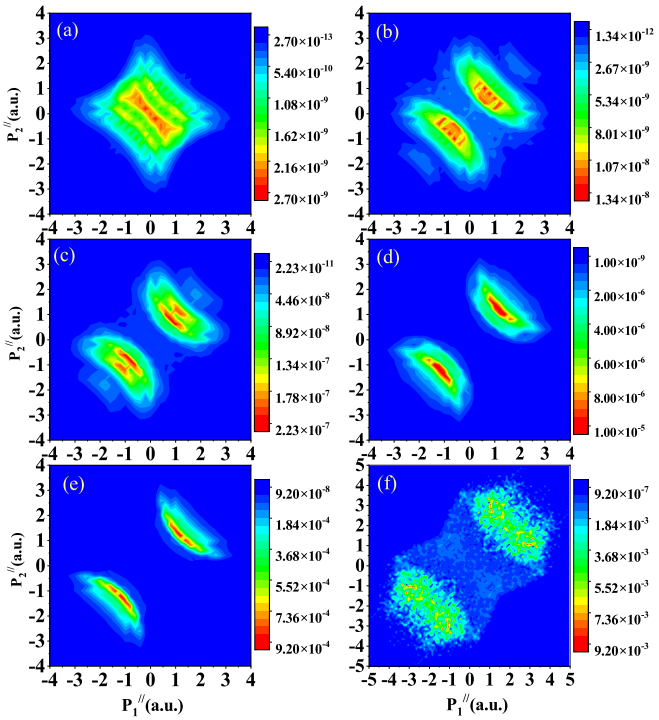


FIG. 2. Correlated electron momentum distribution as a function of the momentum components $p_1^{\parallel}$ and $p_2^{\parallel}$ parallel to the polarization direction obtained using the (a) second-order, (b) third-order, (c) fourth-order, (d) fifth-order, and (e) sixth-order terms of the $S$-matrix expansion and (f) derived from the semiclassical model.

Figure 2 presents the correlated electron momentum distributions calculated by the second- to sixth-order terms of the $S$-matrix expansion as well as the result of the semiclassical model [34–36] for comparison. We display the results of the second- to sixth-order terms separately in order to see how the distributions change from one order to the next, i.e., we do not add them up as one usually does whenever several Feynman diagrams contribute to the same process. Figure 2(a) shows that the second-order momentum distribution populates all quadrants and is concentrated rather close to the origin. In contrast, Figs. 2(b)–2(e) demonstrate that with increasing order the distributions are more and more located in the first and third quadrants only and their maxima shift away from the origin. It is worth mentioning that the sixth-order distribution, which exhibits the largest parallel momenta, qualitatively agrees with the experimental results presented in Ref. [20]. Figure 2(f) shows that the momentum distribution derived from the semiclassical model also mostly occupies the first and third quadrants with rather large values of the parallel momenta. This is consistent with the sixth-order term but completely different from the result of the second-order term. It is important to consider the magnitudes of the NSDI

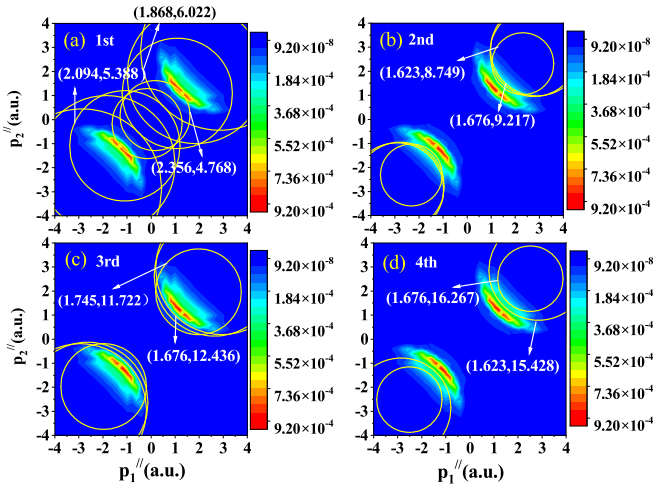


FIG. 3. Each panel repeats the false-color plot of the correlated electron momentum distribution of the sixth-order $S$-matrix expansion as displayed in Fig. 2(e). The various circles in (a)–(d) represent the maximal longitudinal momenta of the electrons released after the (a) first, (b) second, (c) third, and (d) fourth returns of the electron to the core according to the classical simple-man model. Each circle corresponds to a specific ionization time $\omega t_0$, which determines the return time $\omega t_1$ according to the classical simple-man model. For some of the circles, these times are presented in the form $(\omega t_0, \omega t_1)$. The entire region that is classically accessible to electrons after a specified number of returns is given by the envelope of the circles with all possible ionization times. See the text for further explanation.

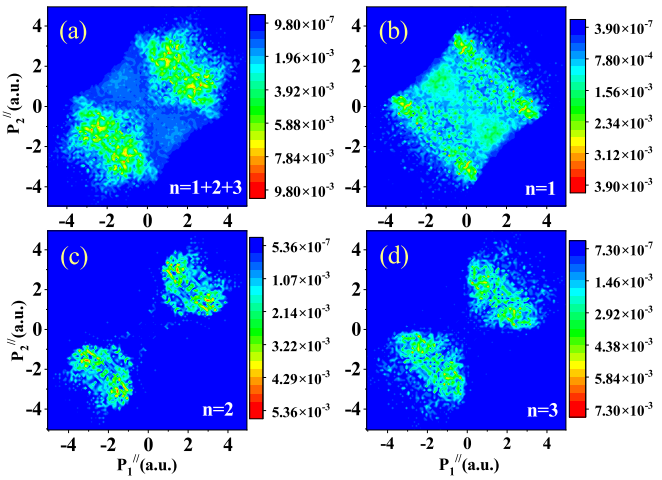


FIG. 4. Correlated electron momentum distributions for NSDI occurring at (b) the first return, (c) the second return, and (d) the third return as well as (a) their sum, calculated from the semiclassical model. (a) is identical to Fig. 2(f).

rates of the various orders: The sixth-order contribution is by far dominant, dwarfing the lower-order contributions by orders of magnitude. We notice in passing that the effect on the momentum-momentum correlation of including more and more Coulomb interactions gives some credence to the introduction of an effective electron-electron interaction as suggested earlier (see, e.g., Refs. [5,67]). In Fig. 3 we present the boundaries of the classically allowed regimes for various trajectories of the tunneled electron that correspond to different return times as calculated from the classical simple-man model [8] for NSDI occurring at the first, second, third, and fourth returns in Figs. 3(a)–3(d), respectively. For some of the curves the pertinent ionization times $\omega t_0$ and return times $\omega t_1$ are indicated. For each return time, the energy left after the second electron has been kicked out is shared as kinetic energy by the two electrons. The condition that both electrons have zero momentum transverse to the laser polarization yields the various circles displayed in Fig. 3. Momenta inside the circles then correspond to the longitudinal momenta of electrons with nonzero transverse momenta. For example, the various yellow circles in Fig. 3(a) enclose the momenta that are classically accessible to electrons that have been liberated at specific times $\omega t_0$ and dislodged the second electron upon the first revisit at the time $\omega t_1$. All plots are symmetrical with respect to the off-diagonal, which reflects the fact that the laser field changes its sign upon $\omega t \to \omega t + \pi$ so that the electron momenta change signs as well. The complete classical boundary for double ionization at the first revisit is given by the envelope of all these curves. We notice that this envelope encloses a simply connected region, in agreement with the $S$-matrix result exhibited in Fig. 2(a). The circles in Figs. 3(b)–3(d) depict the same situation for the second, third, and fourth returns. Evidently, the resulting regions are no longer connected, in agreement with the distributions shown in Figs. 2(b)–2(d). The radii of the circles corresponding to the later returns are smaller because the maximal return energies of the later returns are smaller (the maximal energies that the later returns can acquire converge to $8U_p$ in the simple-man model).

For comparison, in Fig. 4 we display the correlated electron momentum distribution for the first, second, and third return trajectories and their sum calculated via the semiclassical model [34,35]. Inspection of both the quantum results (Fig. 2) and the semiclassical results (Fig. 4) shows that the large momenta in the correlation distributions in the first and third quadrants mainly come from the contributions of the later returns, i.e., from the multiple-return collision NSDI processes [68]. This is a clear indication that these multiple-return processes are enhanced, i.e., the Coulomb focusing effect of the ionized-electron wave packet due to the ion is taken into account by the high-order $S$-matrix theory.

As an interlude, to better understand the magnitudes and shapes of the higher-order contributions of the $S$-matrix expansion, we will analyze the above-threshold ionization (ATI) spectrum of the first-ionized electron as it would be if it were not interacting with the second electron. The corresponding $S$-matrix formalism of ATI is reproduced in the Appendix.

Figure 5 exhibits the ATI photoelectron energy spectrum (PES) for emission in the field direction without interaction with the core (black dotted line), the spectrum if one interaction with the core is included (blue dashed line), and the spectra of electrons that are required to interact twice (green dash–double-dotted line), three times (orange dash-dotted line), and four times (red solid line). The lowest-order term reproduces the well-known direct-electron spectrum with its cutoff around $2U_p$. All higher-order terms exhibit the rescattering plateau. Remarkably, all higher-order terms have exactly the same cutoff energy of about $10U_p$ and more or

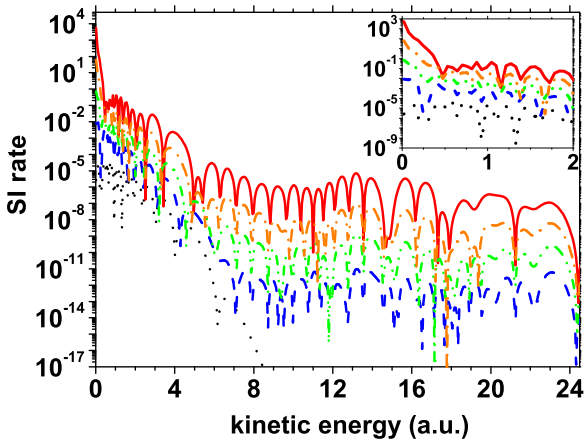


FIG. 5. The ATI photoelectron energy $E_p$ spectrum of the first-ionized electron in the field direction without interaction between the electron and the core (black dotted line), after the electron interacts with the core once (blue dashed line), twice (green dash–double-dotted line), three times (orange dash-dotted line), and four times (red solid line). The ponderomotive energy of the laser field with an intensity of $1.05 \times 10^{15}$ W/cm$^2$ and a wavelength of 800 nm is $U_p = 2.29$ a.u. The inset displays the low-energy spectrum with expanded energy scale. Here SI denotes single ionization.

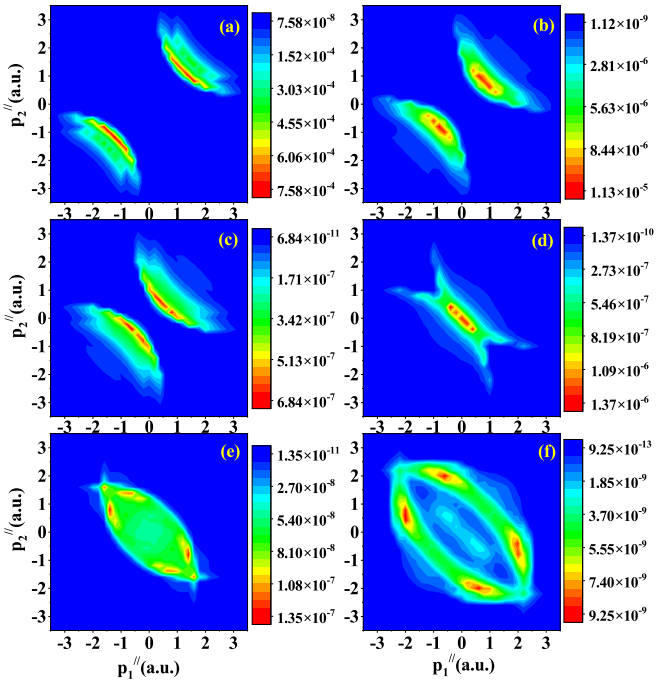


FIG. 6. Correlated electron momentum distributions of the sixth-order term of the *S*-matrix expansion for different ATI energies $E_p$ of the first-ionized electron interaction, where (a) $E_p = 0.02$ a.u., (b) $E_p = 0.25$ a.u., (c) $E_p = 0.53$ a.u., (d) $E_p = 1.1$ a.u., (e) $E_p = 2.24$ a.u., and (f) $E_p = 4.52$ a.u. Note the very different color codes in the various panels.

less the same shape, but the yield dramatically increases from one order to the next. Within the plateau, for four interactions the yield is about four orders of magnitude higher than for just one interaction (standard high-order ATI). For the direct electrons, this enhancement, which comes with an increasing number of electron-core interactions, is not that high but is still substantial. For very low electron energies below 0.5 a.u. ($0.22U_p$), the enhancement increases again. This is possibly related to higher-order contributions to the LES. However, for the relatively short wavelength of 800 nm, the LES is not very pronounced.

We notice that there are three distinct effects that contribute to the overall increase of the yield with an increasing number of interactions. The Coulomb forward-scattering cross section is divergent; hence, any additional such interaction substantially increases the yield without affecting much the shape of the spectrum. Spreading of the electronic wave packet tends to reduce the contribution of higher orders. In contrast, Coulomb refocusing may occur, which enhances the yield.

It is worth emphasizing that the higher-order terms (two or more interactions with the core potential) still observe a cutoff around $10U_p$, while the cutoffs of the longer orbits, i.e., those that rescatter only once but upon a revisit later than the first, are around $8U_p$ [42]. Doing a saddle-point analysis, we find indications that this is explained by interaction events in the forward direction that occur immediately after the release. If so, the final rescattering that kicks out the bound electron takes place at about the same time as in the lowest order. Only rescatterings at this time are able to accelerate electrons up to $10U_p$. A separate investigation of this is left for future work.

The SFA is not normally utilized to obtain absolute numbers for the total ionization rates, only the shape of the electron momentum spectrum. Hence, one should consider the ratios of electrons emitted with different energies. Comparing the emission rates at energies of 2 and 10 a.u., the ratio is about $10^7$ for the first-order interaction (blue dashed line in Fig. 5), while it is $10^3$ with four additional interactions (red solid line). The latter value is in much better agreement with experimental data. The additional strong enhancement of the very-low-energy part of the spectrum deserves special analysis, which is beyond the scope of the present paper.

Next we continue our analysis of the electron momentum correlation distributions by calculating the sixth-order term for various different energies $E_p = p^2/2$ of the first-ionized electron preceding its interaction with the second electron. The solid angle of the momentum $\mathbf{p}$ is integrated over in Eq. (7) and the results are presented in Fig. 6. When this energy is very low (as low as 0.02 a.u.) according to Fig. 6(a) the momentum distribution is almost entirely located in the first and third quadrants with its maxima at relatively high momenta close to the diagonal. As the energy $E_p$ increases, the momentum distribution shifts towards lower parallel momenta and starts spilling into the second and fourth quadrants. At $E_p = 1.1$ a.u., as shown in Fig. 6(d), the distribution has essentially moved to the second and fourth quadrants, with the momenta very close to the origin. However, as the energy $E_p$ continues to increase, the distribution expands again to occupy a much wider region with its maxima remaining in the second and fourth quadrants. It is crucial to note that the lowest energy ($E_p = 0.02$ a.u.) makes by far the greatest contribution. With increasing $E_p$, the contribution to the momentum distribution quickly decreases (cf. the color code of

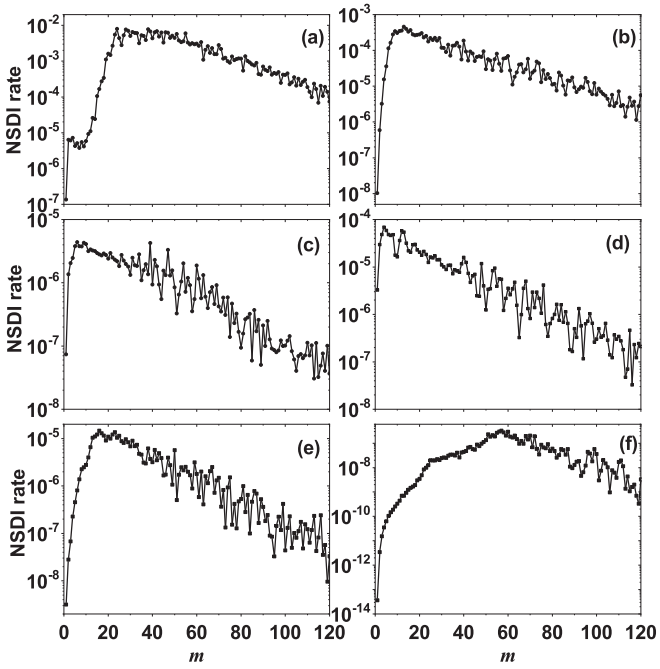


FIG. 7. NSDI rate according to the sixth-order term as a function of $m$, which is the photon number in excess of the minimum needed to be absorbed for double ionization, for different emitted energies $E_p$ of the first-ionized electron without the interaction with the second electron: (a) $E_p = 0.02$ a.u., (b) $E_p = 0.25$ a.u., (c) $E_p = 0.53$ a.u., (d) $E_p = 1.1$ a.u., (e) $E_p = 2.24$ a.u., and (f) $E_p = 4.52$ a.u. Note the different scales of the NSDI rates in the various panels.

the various panels). It is for this reason that the momentum distribution that incorporates all the energies $E_p$ [cf. Fig. 2(e)] is very similar to the one that only contains the lowest energy [cf. Fig. 6(a)]. We conclude that the change of the momentum correlation when going to higher and higher orders in the $S$-matrix can be attributed to the significant enhancement of the very-low-energy part of the ATI photoelectron spectrum (cf. the inset of Fig. 5) with increasing order, which is due to the interaction between the ionic Coulomb potential and the first-ionized electron.

Figure 6 shows that the NSDI yield is highest and the momenta of the final electrons are largest for the case when the corresponding ATI electron has very low energy $E_p$ at the detector. For an explanation, in Fig. 7 we plot the NSDI rate calculated for the sixth-order term as a function of the absorbed photon number $m = 1, 2, \ldots$ in excess of the minimal number required for double ionization, which was introduced below Eq. (13). The panels are for various energies $E_p$ as given in the caption, ranging from very low ($E_p = 0.02$ a.u.) to moderately high ($E_p = 4.52$ a.u. $= 1.96U_p$). In all cases, the NSDI rate first increases and then decreases as a function of $m$. However, the position of its maximum decreases from $m = 23$ to $m = 3$ when $E_p$ increases from 0.02 a.u. to 1.1 a.u., while it again increases from $m = 16$ to $m = 57$ when $E_p$ increases from 2.24 a.u. to 4.52 a.u. This allows us to understand the behavior of the momentum distributions in Fig. 6, which with increasing energy $E_p$ first contract towards the origin and then expand again. If the NSDI rate in Fig. 7 peaks at a large photon number $m$, the total number of absorbed photons for double ionization is relatively large, and the energy left over after both electrons have been liberated is still relatively large, resulting in higher parallel momenta of the two electrons. Conversely, if the NSDI rate peaks at low photon numbers $m$, little energy is left for the two freed electrons. In particular, as shown in Fig. 7(d), for $E_p = 1.1$ a.u., the position of the maximum of the NSDI rate drops to $m = 3$, so the momenta are concentrated very close to the origin. With $E_p$ again increasing, the NSDI rate peaks at larger $m$ and the electrons' final momenta increase again.

It must be emphasized that the velocity gauge is adopted in the present theory and the transition matrix is calculated in the frequency domain. Usually, in the context of length gauge, the time domain is applicable. If, in addition, the saddle-point evaluation is utilized, a transparent physical picture emerges, which allows one to follow the electron dynamics along (quantum) trajectories. In that description, the first electron just preceding the recollision has sufficient kinetic energy to overcome the ionization potential of the second electron and to dislodge it [5,6]. In contrast, in the frequency domain of the velocity-gauge theory, we have no control of the temporal evolution of the double-ionization process. However, we can state that the dominant contribution to double ionization comes from those first-ionized electrons that, had they not interacted with the second electron, would have reached the continuum with very low energy.

The comparison of Figs. 2(e) and 6 suggests the best agreement for the very lowest energy of the first-ionized electron [Fig. 6(a)], which also quantitatively makes the dominant contribution. In the first-electron ATI spectrum of Fig. 5, for all energies and especially for very low energy the contribution of four Coulomb interactions (represented by the red solid line) is by far dominant, in agreement with Fig. 2. When the ATI energy of the first-ionized electron is low, the extra energy of the absorbed photons after overcoming the ionization potential tends to be shared equally by the two electrons, leading to maxima close to the diagonal in the correlation distributions shown in Figs. 6(a)–6(c). In contrast, when the ATI energy is high, the extra energy tends to be acquired unequally, resulting in maxima located far away from the diagonal, even located in the second and fourth quadrants as shown in Figs. 6(e) and 6(f). These are features typical of a Coulomb collision. They have also been observed in the time-domain treatment of NSDI [40,68].

Finally, in Fig. 8 we analyze how the various terms included in the transition amplitude (7) affect the dependence of the NSDI rate on the number $m$ of excess photons. According to Eqs. (7)–(12), the NSDI rate is determined by the Bessel function $J_{N-M}(\boldsymbol{\alpha}\cdot(\mathbf{p}_1+\mathbf{p}_2-\mathbf{p}), -\frac{z}{2})$ and the three factors $V_{\mathbf{p}_2\mathbf{p}_1,j\mathbf{p}}$, $V_{j,i}$, and $T^{(M)}(\mathbf{p})$. Except for the factor $V_{j,i}$, the other two factors and the Bessel function all depend on the photon number $m$. In the following, we will analyze this dependence.

First, to study the effect of $m$ on the Bessel function, we set the values of the other two factors to one. In Fig. 8(a) we plot the NSDI rate considering only the effect of the Bessel function as a function of $m$ for different $E_p$. As $m$ increases, the NSDI rate first increases and then becomes flat for all values of $E_p$. The smaller the $E_p$, the slower the increase of the

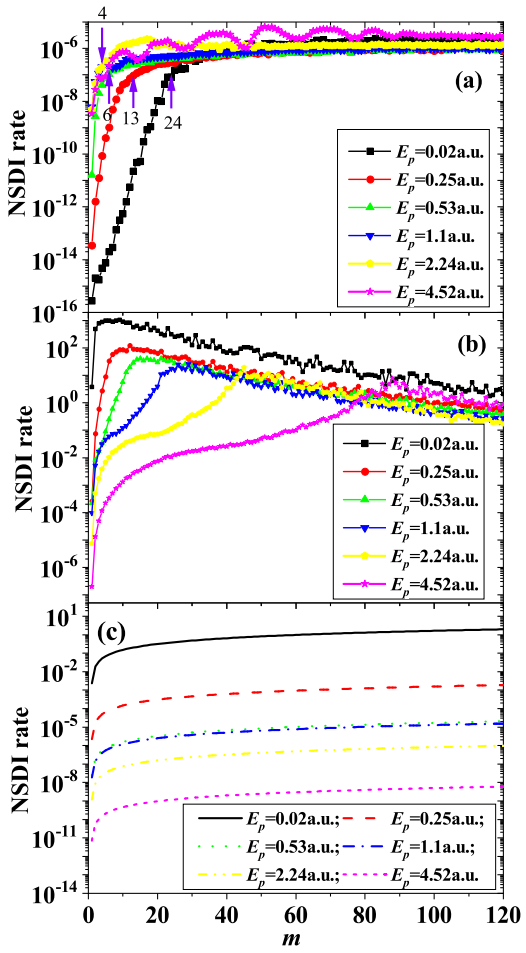


FIG. 8. Calculated NSDI rate as a function of $m$, for different emitted energies $E_p$ of the first-ionized electron, considering the individual effects of three contributing factors (see the text for further details): (a) the Bessel function $J_{N-M}(\boldsymbol{\alpha}\cdot(\mathbf{p}_1+\mathbf{p}_2-\mathbf{p}),-\frac{z}{2})$, (b) the electron-electron collision factor $V_{\mathbf{p}_2\mathbf{p}_1,j\mathbf{p}}$, and (c) the factor of the fourth-return-collision single ionization $T_6^{(M)}(\mathbf{p})$.

NSDI with $m$. The value of $m$ where the curve becomes flat decreases from 24 to 13 to 6 to 4 for $E_p = 0.02$, 0.25, 0.53, and 1.1 a.u., respectively, which is consistent with Figs. 7(a)–7(d). When $E_p$ continues to increase, this value of $m$ remains almost unchanged. Second, in Fig. 8(b) we consider the effect of only the electron-electron collision factor $V_{\mathbf{p}_2\mathbf{p}_1,j\mathbf{p}}$. We find that the NSDI rate first increases and then decreases as $m$ increases. The peak position of the curve moves towards larger $m$ with increasing $E_p$. Third, in Fig. 8(c) we consider the effect of only the factor $T_6^{(M)}(\mathbf{p})$, which takes into account four interactions between the first-ionized electron and the core. Initially, with increasing $m$ the NSDI rate increases rapidly and then more and more slowly. Considering these three factors, the positions of the maxima of the NSDI rates in Fig. 7 are mainly determined by the first two factors. When $E_p$ is relatively small, the contribution of the Bessel function increases more slowly than that of the electron-electron collision factor at small $m$ as shown in Figs. 8(a) and 8(b). Therefore, for small $E_p$ the position of the maximum of the NSDI rate is mainly determined by the Bessel function. In contrast, when $E_p$ is relatively large, the electron-electron collision factor increases more slowly than the Bessel function at small $m$. As a result, for large $E_p$ the position of the maximum of the NSDI rate is mainly determined by the electron-electron collision factor. In addition, one can find that the distribution in Fig. 6 is also mainly determined by the first two factors (the Bessel function and the electron-electron collision factor). Since the maximum of the Bessel function increases with increasing $E_p$ [see Fig. 8(a)] while the electron-electron collision factor decreases and this behavior is more or less the same regardless of the value of $E_p$, the contributions of different $E_p$ to the NSDI rate are of the same order if only these two factors are considered. Therefore, the dominant role of very low $E_p$ mainly comes from the significant enhancement of very low electron energy in the ATI spectrum shown in Fig. 5. In the time domain, this enhancement can be attributed to multiple collisions between the electron and the ionic Coulomb potential, which can be understood as the Coulomb focusing effect, which enhances the multiple-return trajectories.

The question remains of what will happen if one goes to higher and higher order in the $S$-matrix expansion. In principle, the infinite series needs to be summed up to fully take into account the effect of the ionic Coulomb potential on the dynamics of the first-ionized electron. Convergence problems then arise both for each individual term and for the sum since, for the long-range Coulomb potential, the higher-order terms are larger than the lower-order terms (see the PESs in Figs. 2 and 5). This is an open question, which remains beyond the scope of the present paper. However, one may argue that in practice only the highest-order term (the sixth-order term in this paper) is needed to calculate the correlation distribution, that is, terms of still higher orders will not noticeably change the shape of the distribution. For higher-order terms, e.g., the seventh-order term, the very-low-energy region of the PES of the first electron will be even larger than that for the sixth-order term; however, this will affect only the absolute magnitude of the NSDI rate but not the distribution.

## IV. CONCLUSION

We have extended the analysis of nonsequential double ionization based on a Feynman-diagram expansion of the $S$ matrix by including higher-order diagrams that describe up to four Coulomb interactions between the first-ionized electron and the core, the second electron still being bound. While this is only a subset of all of the contributing Feynman diagrams, it reveals a remarkable tendency: With an increasing number of Coulomb interactions, the distribution of the momentum components parallel to the laser field drastically changes. The lowest order, i.e., the customary diagram, which does not incorporate any such interaction, yields a distribution populating all four quadrants and mostly concentrated in the second and fourth quadrants rather close to the origin. Including more and more Coulomb interactions has the effect of shifting the distribution into the first and third quadrants, to larger momenta, and closer to the diagonal. This tendency is most pronounced for the highest-order term that we considered, which allowed for four Coulomb interactions between the first-ionized electron and the core. The resulting momentum-momentum correlation diagram is

similar to the results of the semiclassical rescattering model and to experimental observations. Performing a corresponding $S$-matrix expansion for above-threshold ionization, we observed a strong enhancement of the total ionization yield and especially of the yield of electrons with very low energy. We showed that these two effects in ATI and in NSDI are related: The dominance of first-ionized electrons having very low energy before their final interaction with the second electron is responsible for the shift towards relatively high parallel final momenta of the liberated electrons in NSDI. We have shown that higher orders of the $S$-matrix expansion do lead to pronounced effects that very noticeably change the agreement or disagreement between theory and experiment. This is an important insight for intense-laser-atom physics in general.

## ACKNOWLEDGMENTS

This work was supported by the National Key Research and Development Program of China (Grant No. 2019YFA0307700) and National Natural Science Foundation of China (Grants No. 61221064, No. 12274300, and No. 12274273).

## APPENDIX: THE $S$-MATRIX EXPANSION FOR SINGLE IONIZATION

In the single-active-electron approximation, the $S$-matrix expansion for ionization into a continuum state with momentum $\mathbf{p}$ is

$$\begin{aligned}(S-1)_{fi} &= T^{(1)} + T^{(2)} + T^{(3)} + \cdots \\ &= -i\int_{-\infty}^{\infty} dt_1 \langle \psi_{\mathbf{p}}^{(V)}(\mathbf{r},t_1)|V_L(t_1)|\phi_i(\mathbf{r},t_1)\rangle + (-i)^2 \\ &\times \int_{-\infty}^{\infty} dt_2 \int_{-\infty}^{t_2} dt_1 \int d^3\mathbf{p}' \langle \psi_{\mathbf{p}}^{(V)}(\mathbf{r},t_2)|V_C|\psi_{\mathbf{p}'}^{(V)}(\mathbf{r},t_2)\rangle\langle \psi_{\mathbf{p}'}^{(V)}(\mathbf{r},t_1)|V_L(t_1)|\phi_i(\mathbf{r},t_1)\rangle + (-i)^3 \\ &\times \int_{-\infty}^{\infty} dt_3 \int_{-\infty}^{t_3} dt_2 \int_{-\infty}^{t_2} dt_1 \int d^3\mathbf{p}' \int d^3\mathbf{p}'' \langle \psi_{\mathbf{p}}^{(V)}(\mathbf{r},t_3)|V_C|\psi_{\mathbf{p}'}^{(V)}(\mathbf{r},t_3)\rangle\langle \psi_{\mathbf{p}'}^{(V)}(\mathbf{r},t_2)|V_C|\psi_{\mathbf{p}''}^{(V)}(\mathbf{r},t_2)\rangle \\ &\times \langle \psi_{\mathbf{p}''}^{(V)}(\mathbf{r},t_1)|V_L(t_1)|\phi_i(\mathbf{r},t_1)\rangle + \cdots, \end{aligned} \tag{A1}$$

where $V_L(t)$ and $V_C$ are the laser-atom interaction and the electron–parent-ion Coulomb interaction (with $Z_{\text{eff}} = \sqrt{2I_{p_1}}$), respectively, as defined in the main text. The atomic ground state is $|\phi_i(\mathbf{r},t)\rangle$ and $|\psi_{\mathbf{p}}^{(V)}(\mathbf{r},t)\rangle$ is the Volkov state with the final electron momentum $\mathbf{p}$. The first term on the right-hand side of the second equality in (A1) of this expansion describes the direct electrons, which do not interact with the binding potential after they have been liberated. The second term allows for just one such rescattering interaction, and each subsequent higher-order term contains one additional interaction $V_C$, with propagation in the presence of the laser field (Volkov propagation) in between.

For the evaluation, we analytically perform the time integral for each term and obtain, as an example, the third term as

$$T^{(3)} = \sum_{n,n',n''}^{\infty} \int p'dp'd\Omega' \int p''dp''d\Omega'' \frac{J_n((\mathbf{p}-\mathbf{p}')\cdot\boldsymbol{\alpha})}{(\mathbf{p}-\mathbf{p}')^2+\kappa^2} \frac{J_{n'}((\mathbf{p}'-\mathbf{p}'')\cdot\boldsymbol{\alpha})}{(\mathbf{p}'-\mathbf{p}'')^2+\kappa^2} J_{n''}\left(\mathbf{p}''\cdot\boldsymbol{\alpha}, -\frac{z}{2}\right)(n''\omega - U_p)\phi_i(\mathbf{p}''), \tag{A2}$$

where

$$\begin{aligned}\frac{p''^2}{2} &= n''\omega - U_p - I_p, \\ \frac{p'^2}{2} &= (n'+n'')\omega - U_p - I_p, \\ \frac{p^2}{2} &= (n+n'+n'')\omega - U_p - I_p. \end{aligned} \tag{A3}$$

To obtain Eqs. (A2) and (A3), we adopted the pole approximation, as described in the main text in connection with Eq. (14). Moreover, to ensure convergence, a screening parameter $\kappa$ was introduced in Eq. (A2).

[1] P. Agostini, F. Fabre, G. Mainfray, G. Petite, and N. K. Rahman, Phys. Rev. Lett. **42**, 1127 (1979).

[2] G. G. Paulus, W. Nicklich, H. Xu, P. Lambropoulos, and H. Walther, Phys. Rev. Lett. **72**, 2851 (1994).

[3] A. D. Shiner, B. E. Schmidt, C. Trallero-Herrero, H. J. Wörner, S. Patchkovskii, P. B. Corkum, J. C. Kieffer, F. Légaré, and D. M. Villeneuve, Nat. Phys. **7**, 464 (2011).

[4] A. I'Huillier, L. A. Lompre, G. Mainfray, and C. Manus, Phys. Rev. A **27**, 2503 (1983).

[5] W. Becker, X. J. Liu, P. J. Ho, and J. H. Eberly, Rev. Mod. Phys. **84**, 1011 (2012).

[6] C. Figueira de Morisson Faria and X. Liu, J. Mod. Opt. **58**, 1076 (2011).

[7] D. N. Fittinghoff, P. R. Bolton, B. Chang, and K. C. Kulander, Phys. Rev. Lett. **69**, 2642 (1992).

[8] P. B. Corkum, Phys. Rev. Lett. **71**, 1994 (1993).

[9] M. Y. Kuchiev, J. Phys. B **28**, 5093 (1995).

[10] A. Becker and F. H. M. Faisal, J. Phys. B **29**, L197 (1996).

[11] J. Ullrich, R. Moshammer, R. Dörner, O. Jagutzki, V. Mergel, H. Schmidt-Böcking, and L. Spielberger, J. Phys. B **30**, 2917 (1997).

[12] T. Weber, M. Weckenbrock, A. Staudte, L. Spielberger, O. Jagutzki, V. Mergel, F. Afaneh, G. Urbasch, M. Vollmer, H. Giessen, and R. Dörner, Phys. Rev. Lett. **84**, 443 (2000).

[13] R. Moshammer, B. Feuerstein, W. Schmitt, A. Dorn, C. D. Schröter, J. Ullrich, H. Rottke, C. Trump, M. Wittmann, G. Korn, K. Hoffmann, and W. Sandner, Phys. Rev. Lett. **84**, 447 (2000).

[14] T. Weber, M. Weckenbrock, A. Staudte, L. Spielberger, O. Jagutzki, V. Mergel, F. Afaneh, G. Urbasch, M. Vollmer, H. Giessen, and R. Dörner, J. Phys. B **33**, L127 (2000).

[15] V. L. B. de Jesus, B. Feuerstein, K. Zrost, D. Fischer, A. Rudenko, F. Afaneh, C. D. Schröter, R. Moshammer, and J. Ullrich, J. Phys. B **37**, L161 (2004).

[16] T. Weber, H. Giessen, M. Weckenbrock, G. Urbasch, A. Staudte, L. Spielberger, O. Jagutzki, V. Mergel, M. Vollmer, and R. Dörner, Nature (London) **405**, 658 (2000).

[17] B. Feuerstein, R. Moshammer, D. Fischer, A. Dorn, C. D. Schröter, J. Deipenwisch, J. R. Crespo Lopez-Urrutia, C. Höhr, P. Neumayer, J. Ullrich, H. Rottke, C. Trump, M. Wittmann, G. Korn, and W. Sandner, Phys. Rev. Lett. **87**, 043003 (2001).

[18] M. Weckenbrock, M. Hattass, A. Czasch, O. Jagutzki, L. Schmidt, T. Weber, H. Roskos, T. Löffler, M. Thomson, and R. Dörner, J. Phys. B **34**, L449 (2001).

[19] R. Moshammer, B. Feuerstein, J. Crespo Lopez-Urrutia, J. Deipenwisch, A. Dorn, D. Fischer, C. Höhr, P. Neumayer, C. D. Schröter, J. Ullrich, H. Rottke, C. Trump, M. Wittmann, G. Korn, and W. Sandner, Phys. Rev. A **65**, 035401 (2002).

[20] R. Moshammer, J. Ullrich, B. Feuerstein, D. Fischer, A. Dorn, C. D. Schröter, J. R. Crespo Lopez-Urrutia, C. Höhr, H. Rottke, C. Trump, M. Wittmann, G. Korn, K. Hoffmann, and W. Sandner, J. Phys. B **36**, L113 (2003).

[21] R. Kopold, W. Becker, H. Rottke, and W. Sandner, Phys. Rev. Lett. **85**, 3781 (2000).

[22] A. Staudte, C. Ruiz, M. Schöffler, S. Schössler, D. Zeidler, T. Weber, M. Meckel, D. M. Villeneuve, P. B. Corkum, A. Becker, and R. Dörner, Phys. Rev. Lett. **99**, 263002 (2007).

[23] A. Rudenko, V. L. B. de Jesus, T. Ergler, K. Zrost, B. Feuerstein, C. D. Schröter, R. Moshammer, and J. Ullrich, Phys. Rev. Lett. **99**, 263003 (2007).

[24] C. Figueira de Morisson Faria, X. Liu, W. Becker, and H. Schomerus, Phys. Rev. A **69**, 021402(R) (2004).

[25] S. L. Haan, J. S. Van Dyke, and Z. S. Smith, Phys. Rev. Lett. **101**, 113001 (2008).

[26] D. F. Ye, X. Liu, and J. Liu, Phys. Rev. Lett. **101**, 233003 (2008).

[27] Z. J. Chen, Y. Q. Liang, and C. D. Lin, Phys. Rev. Lett. **104**, 253201 (2010).

[28] S. V. Popruzhenko, P. A. Korneev, S. P. Goreslavski, and W. Becker, Phys. Rev. Lett. **89**, 023001 (2002).

[29] X. L. Hao, J. Chen, W. D. Li, B. Wang, X. Wang, and W. Becker, Phys. Rev. Lett. **112**, 073002 (2014).

[30] A. S. Maxwell and C. Figueira de Morisson Faria, Phys. Rev. Lett. **116**, 143001 (2016).

[31] W. Quan, X. L. Hao, Y. L. Wang, Y. J. Chen, S. G. Yu, S. P. Xu, Z. L. Xiao, R. P. Sun, X. Y. Lai, S. L. Hu, M. Q. Liu, Z. Shu, X. D. Wang, W. D. Li, W. Becker, X. J. Liu, and J. Chen, Phys. Rev. A **96**, 032511 (2017).

[32] X. L. Hao, Y. X. Bai, C. Li, J. Y. Zhang, W. D. Li, W. F. Yang, M. Q. Liu, and J. Chen, Commun. Phys. **5**, 31 (2022).

[33] J. S. Parker, L. R. Moore, K. J. Meharg, D. Dundas, and K. T. Taylor, J. Phys. B **34**, L69 (2001).

[34] J. Chen, J. Liu, L. B. Fu, and W. M. Zheng, Phys. Rev. A **63**, 011404(R) (2000).

[35] L. B. Fu, J. Liu, J. Chen, and S. G. Chen, Phys. Rev. A **63**, 043416 (2001).

[36] X. L. Hao, G. Q. Wang, X. Y. Jia, W. D. Li, J. Liu, and J. Chen, Phys. Rev. A **80**, 023408 (2009).

[37] R. Panfili, S. L. Haan, and J. H. Eberly, Phys. Rev. Lett. **89**, 113001 (2002).

[38] A. Becker and F. H. M. Faisal, Phys. Rev. Lett. **84**, 3546 (2000).

[39] A. Becker and F. H. M. Faisal, Phys. Rev. Lett. **89**, 193003 (2002).

[40] C. Figueira de Morisson Faria, H. Schomerus, X. Liu, and W. Becker, Phys. Rev. A **69**, 043405 (2004).

[41] C. Figueira de Morisson Faria, T. Shaaran, X. Liu, and W. Yang, Phys. Rev. A **78**, 043407 (2008).

[42] For a review see, e.g., W. Becker, F. Grasbon, R. Kopold, D. B. Milošević, G. G. Paulus, and H. Walther, Adv. At. Mol. Opt. Phys. **48**, 35 (2002).

[43] L. V. Keldysh, Ionization in the field of a strong electromagnetic wave, Zh. Eksp. Teor. Fiz. **47**, 1945 (1964) [Sov. Phys. JETP **20**, 1307 (1965)].

[44] H. R. Reiss, Phys. Rev. A **22**, 1786 (1980).

[45] F. M. H. Faisal, J. Phys. B **6**, L89 (1973).

[46] R. Moshammer, J. Ullrich, B. Feuerstein, D. Fischer, A. Dorn, C. D. Schröter, J. R. Crespo Lopez-Urrutia, C. Hoehr, H. Rottke, C. Trump, M. Wittmann, G. Korn, and W. Sandner, Phys. Rev. Lett. **91**, 113002 (2003).

[47] C. I. Blaga, F. Catoire, P. Colosimo, G. G. Paulus, H. G. Muller, P. Agostini, and L. F. DiMauro, Nat. Phys. **5**, 335 (2009).

[48] J. Chen and C. H. Nam, Phys. Rev. A **66**, 053415 (2002).

[49] W. Quan, Z. Lin, M. Wu, H. Kang, H. Liu, X. Liu, J. Chen, J. Liu, X. T. He, S. G. Chen, H. Xiong, L. Guo, H. Xu, Y. Fu, Y. Cheng, and Z. Z. Xu, Phys. Rev. Lett. **103**, 093001 (2009).

[50] C. Y. Wu, Y. D. Yang, Y. Q. Liu, Q. H. Gong, M. Y. Wu, X. Liu, X. L. Hao, W. D. Li, X. T. He, and J. Chen, Phys. Rev. Lett. **109**, 043001 (2012).

[51] J. Dura, N. Camus, A. Thai, A. Britz, M. Hemmer, M. Baudisch, A. Senftleben, C. D. Schröter, J. Ullrich, R. Moshammer, and J. Biegert, Sci. Rep. **3**, 2675 (2013).

[52] W. Becker, S. P. Goreslavski, D. B. Milošević, and G. G. Paulus, J. Phys. B **47**, 204022 (2014).

[53] L. Guo, S. S. Han, X. Liu, Y. Cheng, Z. Z. Xu, J. Fan, J. Chen, S. G. Chen, W. Becker, C. I. Blaga, A. D. DiChiara, E. Sistrunk, P. Agostini, and L. F. DiMauro, Phys. Rev. Lett. **110**, 013001 (2013).

[54] B. Wolter, C. Lemell, M. Baudisch, M. G. Pullen, X.-M. Tong, M. Hemmer, A. Senftleben, C. D. Schröter, J. Ullrich, R. Moshammer, J. Biegert, and J. Burgdörfer, Phys. Rev. A **90**, 063424 (2014).

[55] W. Quan, X. L. Hao, Y. J. Chen, S. G. Yu, S. P. Xu, Y. L. Wang, R. P. Sun, X. Y. Lai, C. Y. Wu, Q. H. Gong, X. T. He, X. J. Liu, and J. Chen, Sci. Rep. **6**, 27108 (2016).

[56] L. Guo, J. Chen, J. Liu, and Y. Q. Gu, Phys. Rev. A **77**, 033413 (2008).

[57] C. Liu and K. Z. Hatsagortsyan, Phys. Rev. Lett. **105**, 113003 (2010).

[58] T. M. Yan, S. V. Popruzhenko, M. J. J. Vrakking, and D. Bauer, Phys. Rev. Lett. **105**, 253002 (2010).

[59] A. Kästner, U. Saalmann, and J. M. Rost, Phys. Rev. Lett. **108**, 033201 (2012).

[60] X. Y. Jia, X. L. Hao, D. H. Fan, W. D. Li, S. L. Hu, and J. Chen, J. Phys. B **52**, 065601 (2019).

[61] T. Brabec, M. Y. Ivanov, and P. B. Corkum, Phys. Rev. A **54**, R2551(R) (1996).

[62] S. A. Kelvich, W. Becker, and S. P. Goreslavski, Phys. Rev. A **93**, 033411 (2016); **96**, 023427 (2017).

[63] L. Guo, X. Y. Jia, W. Becker, and J. Chen (unpublished).

[64] C. Figueira de Morisson Faria and A. S. Maxwell, Rep. Prog. Phys. **83**, 034401 (2020).

[65] V. I. Usachenko, V. A. Pazdzersky, and J. K. McIver, Phys. Rev. A **69**, 013406 (2004).

[66] C. Figueira de Morisson Faria and M. Lewenstein, J. Phys. B **38**, 3251 (2005).

[67] S. P. Goreslavskii, S. V. Popruzhenko, R. Kopold, and W. Becker, Phys. Rev. A **64**, 053402 (2001).

[68] X. Y. Jia, X. L. Hao, D. H. Fan, W. D. Li, and J. Chen, Phys. Rev. A **88**, 033402 (2013).